Submitted: 22 January 2018

Published online in 'accepted manuscript' format: 18 June 2018

Manuscript title: Experiments and Dimensional Analysis of Contaminated Clay Soils

Authors: Amin Soltani[1], A.R. Estabragh[2], Abbas Taheri[1], An Deng[1], Jay N. Meegoda[3]

Affiliations: [1]School of Civil, Environmental and Mining Engineering, The University of Adelaide, Adelaide, SA 5005, Australia. [2]Faculty of Soil and Water Engineering, University of Tehran, PO BOX 4411, Karaj 31587–77871, Iran. [3]Department of Civil and Environmental Engineering, New Jersey Institute of Technology, Newark, NJ 07102, USA.

Corresponding author: Amin Soltani, School of Civil, Environmental and Mining Engineering, The University of Adelaide, Adelaide, SA 5005, Australia. Tel.: +61–8–83132830

E-mail: Amin.Soltani@adelaide.edu.au

Abstract

An experimental program was developed to investigate the influence of three viscous–dominant contaminants on the stress–strain response of clay soils. Four degrees of contamination (by weight), i.e. C_c=2%, 4%, 6% and 8%, were examined. Natural and contaminated samples were prepared at their respective Proctor optimum condition, and further subjected to unconfined compression tests. The dimensional analysis concept was implemented to quantify the stress–strain response. A sensitivity analysis with respect to the proposed dimensional models was also performed to examine the impact of various contamination scenarios on the strength properties. Lubrication at particle contact level caused by the viscous nature of the contaminant agent portrayed a significant role in describing the stress–strain response. The stress–strain relationship was adversely affected by contamination. The peak strength and stiffness were inversely related to contaminant viscosity μ_c and C_c, with the former representing a more dominant role. An increase in μ_c and/or C_c, however, promoted a notable improvement in the ductility. The predictive capacity of the proposed dimensional models was examined and validated by statistical techniques. The proposed models contain a limited number of fitting parameters, which can be calibrated by minimal experimental effort and hence implemented for predictive purposes.

Notation

C_c	degree of contamination (=W_c/W_s)
D	dielectric constant
E	Young's modulus or modulus of elasticity
LL	liquid limit
MAPE	mean absolute percentage error (in %)
NRMSE	normalized root mean squares error (in %)
$P(x_i)^-$	likelihood of decrease in y as a result of increase in x_i
$P(x_i)^+$	likelihood of increase in y as a result of increase in x_i
PI	plasticity index (=$LL–PL$)
PL	plastic limit
q_u	unconfined compressive strength
R^2	coefficient of determination
RMSE	root mean squares error
$S(x_i)$	sensitivity of y with respect to variations in x_i
SSA	specific surface area
W_c	weight of contaminant agent
W_s	weight of dry soil
W_w	weight of water
x_i	independent variable (=μ_c and C_c)
y	dependent variable (=q_u or E)
α_0, α_1 and α_2	fitting parameters with respect to the proposed dimensional model for q_u
β_0, β_1 and β_2	fitting parameters with respect to the proposed dimensional model for E
γ_{d0}	initial dry unit weight

γ_{dmax}	maximum dry unit weight
ε_u	axial strain at failure
$\eta(x_i)^-$	negative magnitude on y caused by increase in x_i
$\eta(x_i)^+$	positive magnitude on y caused by increase in x_i
μ^*	dimensionless viscosity number
μ_c	absolute viscosity of the contaminant agent
μ_w	absolute viscosity of water
π_0	dependent π term
π_1, π_2 and π_3	independent π terms
ω'_0	initial moisture content (=$[W_c+W_w]/W_s$)
ω'_{opt}	optimum moisture content
ω_0	initial water content (=W_w/W_s)
ω_{opt}	optimum water content

Introduction

Studying the mechanical response of soils under the influence of contamination has been a subject of major interest for the past few decades. Extensive soil contamination has taken place in the past and still continues as a consequence of common industrial and agricultural activities (Meegoda et al. 1996; Meegoda et al. 1998; Ratnaweera and Meegoda 2006). From a geotechnical perspective, contaminants can be classified into two categories based on their originating composition, i.e. inorganic and organic. Inorganic contaminants are defined as mineral–based compounds such as metals, which naturally occur in the geology or are caused by human activities through mining and agriculture. Organic contaminants, however, consist of carbon–based chemicals (e.g. petrochemical products, industrial solvents, detergents and pesticides), which mainly originate from crude oil refinement. The occurrence of organic contaminants in the soil can be a consequence of agricultural operations as well as leakage from underground or aboveground storage tanks and accidental spills (Khamehchiyan et al. 2007; Estabragh et al. 2014). Exposure to leachate produced from the decomposition of municipal, industrial and clinical waste, particularly in landfill sites, can also be a source of severe contamination (Kjeldsen et al. 2002; Moavenian and Yasrobi 2008).

The mechanical response of a contaminated soil not only depends on the local environment, but is also strongly influenced by factors such as particle size, bonding characteristics among particles, and ion exchange capacity (Fang 1997). In this context, Fang (1997) suggested an index parameter, referred to as the pollution sensitivity index PSI, and introduced a framework for the classification of contamination vulnerability with respect to the soil's particle size distribution. The PSI ranges between 0 and 1, with higher values indicating a higher vulnerability to contamination. For gravels and sands, the PSI ranges between 0.05 and 0.10 (i.e. very low to low sensitivity), while $0.1<PSI<0.5$ has been suggested for silts (i.e. medium

sensitivity). Clays are recognized with high to very high sensitivity, and correspond to 0.5<PSI<0.9. Therefore, fine–grained soils, clays in particular, are more likely to be influenced by contamination, and thus require additional consideration. Depending on the mineralogical composition of the soil exposed to contamination, different mechanical responses could be expected. In the case of clay minerals, for instance, montmorillonite would be more sensitive to contamination compared to illite and kaolinite (Fang 1997). Contamination alters the pore–fluid of a clay soil by partially or fully replacing the original pore–fluid composition with new chemical components. This is often accompanied by a series of short– and long–term physico–chemical interactions, which result in different fabric of soil, and thus different mechanical behavior (Meegoda and Rajapakse 1993; Meegoda et al. 1998; Ratnaweera and Meegoda 2006; Estabragh et al. 2016a).

The need to expand industrial activities, often around urban areas to satisfy demands of a growing population, has placed more soils and lands in jeopardy of contamination if not yet exposed. Shortage of land for development as well as increasing costs associated with construction and raw materials has encouraged maximum utilization of local materials, one being contaminated soils (Benson et al. 1998; Meegoda et al. 1998). Potential applications and/or beneficial reuse of contaminated soils with emphasis on maintaining design criteria, however, requires an in–depth knowledge of the geotechnical properties of these soils. Some of the earlier studies introduced theoretical concepts governing the contamination phenomenon with respect to permeability, compressibility and shear strength (e.g. Michaels and Lin 1954; Mesri and Olson 1971; Sridharan and Venkatappa Rao 1973, 1979; Fernandez and Quigley 1985; Rao and Sridharan 1985; Bowders Jr. and Daniel 1987; Abdul et al. 1990; Meegoda and Rajapakse 1993; Sridharan and Prakash 1999; Chen et al. 2000; Kaya and Fang 2000). These theoretical concepts where further examined by a number of researchers through extensive

experimental investigations covering a variety of testing approaches, soil types and contaminant agents. A summary of the studies on soil contamination is presented in **Table 1**. As demonstrated in the table, the majority of documented studies have mainly addressed either coarse–grained soils or low–plasticity clays. A rather common emphasis on properties such consistency limits, compaction characteristics, permeability, shear strength (by means of direct shear testing) and compressibility can be observed. Other aspects such swelling, bearing capacity and unconfined compressive strength, however, seem to be researched to a lesser degree. In addition, crude oil and other hydrocarbon–related fuels have been the spotlight of nearly all studies, while other equally important organic blends (e.g. alcohol–based blends), which are widely distributed and consumed by human–life, have yet been fully addressed. Furthermore, a fair agreement is not present among the findings of these studies, in what can describe the soil contamination topic as a complex phenomenon demanding further investigation. Where contamination poses no significant threat to the environment (i.e. low degrees of contamination), the application of contaminated soils as a construction material for earthworks, e.g. embankments, backfills and pavements, suggests an attractive and economic scheme (Al-Sanad et al. 1995; Meegoda et al. 1998; Estabragh et al. 2014, 2016a). Considering recent breakthroughs in stabilization of contaminated soils by low inclusions of cementitious agents, e.g. cement, lime and fly–ash, the proposition has gained increased attention among practicing engineers (e.g. Tuncan et al. 2000; Trembley et al. 2002; Al-Rawas et al. 2005; Hassan et al. 2005; Estabragh et al. 2016b, 2016c, 2017).

In this paper, an experimental program was developed to investigate the influence of three viscous–dominant contaminant agents, i.e. glycerol, ethanol and ethylene glycol, on the stress–strain response of two clay soils. An attempt was also made to implement the dimensional analysis concept to quantify the stress–strain response of the contaminated soil. Finally, a

sensitivity analysis with respect to the proposed dimensional models was performed to examine the impact of various contamination scenarios on the shear strength properties.

Experimental work

Materials

Soils

Two clay soils, hereafter referred to as soils A and B, were used for the experimental program. Soil A was characterized as *clay with intermediate plasticity* (CI) in accordance with the Unified Soil Classification System (USCS). Soil B, however, was classified as *clay with high plasticity* (CH). Both of the soils can be classified as neutral substances, which correspond to pH values of 7.9 and 8.3 for soils A and B, respectively. The electrical conductivity (EC) and cation exchange capacity (CEC) were also measured, which resulted in 7.76 dS/m and 15.52 meq/100gr for soil A, and 10.25 dS/m and 17.95 meq/100gr for soil B, respectively. Mechanical properties of the soils, determined as per relevant ASTM standards, are presented in **Table 2**. Soil A had an optimum water content and maximum dry unit weight of 19.05% and 16.71 kN/m^3, respectively. For soil B, these values were measured as 23.40% and 14.95 kN/m^3, respectively.

Contaminants

Three liquids, i.e. glycerol (propane–1,2,3–triol in International Union of Pure and Applied Chemistry or IUPAC), ethanol and ethylene glycol (ethane–1,2–diol in IUPAC), were used as the contaminants. These water–soluble organic compounds, commonly involved as key substances over a variety of industrial activates, have been the subject of extensive production over the past few decades. Major applications of glycerol can be found in the detergents industry as well as pharmaceutical productions. Ethylene glycol is commonly recognized as the raw material in the manufacturing of polyester fibers and polyethylene terephthalate resins. Ethanol,

probably the most well–known in this context, assumes a significant role in almost every major industry including its well–established use for medical applications.

To cover a wide range of desired viscosities, the three contaminant agents were used as diluted solutions with a concentration of 40% (i.e. contaminant to water weight ratio). To avoid structural rearrangements as a result of a varying pore–fluid composition, the electrical conductivity of the contaminant solutions was maintained at EC=8.40×10^{-3} dS/m (i.e. EC of deionized water). This was achieved by adding the required amount of sodium chloride (NaCl) to each solution (Meegoda et al. 1998; Ratnaweera and Meegoda 2006; Estabragh et al. 2014, 2016a). Four degrees of contamination (i.e. contaminant to dry soil weight ratio), i.e. C_c=2%, 4%, 6% and 8%, were examined. The four C_c choices were selected in accordance with the state of New Jersey classification criteria, which recognizes oil contents greater than or equal to 3% as hazardous waste (Meegoda and Ratnaweera 1995). Physical and chemical properties of the contaminant agents (at 40% concentration), as provided by the manufacturer, are presented in **Table 3**. The three contaminant agents can be classified as viscous–dominant, each having an absolute viscosity greater than that of deionized water (i.e. μ_w=0.894 cP). For glycerol, ethanol and ethylene glycol, the absolute viscosity was provided as μ_c=4.310 cP, 2.148 cP and 1.181 cP, respectively.

Method of contamination and sample preparation

The required amount of contaminants corresponding to the desired degrees of contamination, i.e. C_c=2%, 4%, 6% and 8%, by weight was evenly sprayed on 5 kg of spreaded soil. The contaminated soils were then thoroughly mixed by hand in a covered bowl to minimize evaporation. Extensive care was dedicated to pulverize the lumped particles, targeting homogeneity of mixtures. The contaminated mixtures were then enclosed in plastic bags, and stored in a polystyrene container under room temperature conditions. A minimum curing time of

7 days, as suggested in the literature (e.g. Meegoda and Gunasekara 1992; Meegoda and Ratanweera 1995, 2008; Singh et al. 2008; Estabragh et al. 2016b, 2016c), was considered to ensure an even distribution of moisture throughout the soil mass.

Standard Proctor compaction tests were carried out on the natural soil and various contaminated mixtures in accordance with the ASTM D698 standard, and the results are provided in **Table 4**. In general, the greater the contaminant viscosity and/or degree of contamination the higher the maximum dry unit weight and the lower the optimum moisture content, following a monotonic decreasing trend. Such a behavior can be attributed to the viscous character of the contaminant agent which acts as a lubricant, and thus reduces the surface tension of water during compaction. This property facilitates the movement and sliding of particles with much less effort, thereby promoting a higher maximum dry unit weight compared with the natural soil (Meegoda et al. 1998; Park et al. 2006; Soltani et al. 2017a). All samples in this study were prepared by static compaction at their respective optimum moisture content and maximum dry unit weight. A special mold, similar to that described by the authors' in Soltani et al. (2017b), was designed and fabricated from stainless steel to accomplish static compaction. The mold consisted of three sections, i.e. the top collar, the middle section and the bottom collar. The middle section measures 100 mm in height and 50 mm in diameter, and accommodates the sample for the unconfined compression test. The inner surface of the mold was coated with a very thin layer of silicon grease to reduce friction during compaction. The mixtures, either natural or contaminated, were thoroughly mixed with the required amount of water, each mixture having attained its respective optimum moisture content. The mixtures were then compressed in the mold in three layers, each layer having attained its desired maximum dry unit weight. The surface of the first and second compacted layers were scarified to ensure a good

bond between adjacent layers of the mixture. Mechanical properties of the prepared samples including consistency limits and compaction characteristics are summarized in **Table 4**.

Unconfined compression test

Unconfined compression tests were carried out on the natural soil and various contaminated samples, prepared as per **Section 2.2**, in accordance with the ASTM D2166 standard. Samples were compressed by a constant displacement rate of 1 mm/min, as commonly adopted in the literature (e.g. Fatahi et al. 2012; Estabragh et al. 2016b, 2016c, 2017; Soltani et al. 2017a). Axial stress and its corresponding axial strain were recorded during various loading stages to a point in which maximum axial stress required for sample failure (defined as the unconfined compressive strength q_u), and its corresponding axial strain (denoted as ε_u) could be achieved. Slope of the tangent to the initial segment of the stress–strain curve, a measure of the material's stiffness (defined as Young's modulus or modulus of elasticity E), was also measured for the tested samples.

Discussion of test results

The consistency limits, the liquid limit in particular, can be employed to infer the development of soil fabric, and thus arrive at initial inferences on the mechanical performance of contaminated soils (Wroth and Wood 1978; Mitchell and Soga 2005; Kim and Palomino 2009; Soltani et al. 2018a). Based on the results presented in **Table 4**, for a given degree of contamination C_c, an increase in contaminant viscosity μ_c led to a significant decrease in both the liquid limit LL and the plasticity index PI. Similarly, for a given μ_c, an increase in C_c was accompanied by a notable yet less pronounced decrease in LL and PI. Soil A exhibited a liquid limit of LL=43.12%. As a result of C_c=2%, 4%, 6% and 8% ethanol contamination, for instance, LL decreased to 41.73%, 40.11%, 39.47% and 38.03%, respectively. A similar yet more pronounced decreasing trend was

also observed soil B–ethanol mixtures, where *LL* decreased from 85.30% to 81.15%, 78.03%, 77.62% and 74.52% for C_c=2%, 4%, 6% and 8%, respectively. A decrease in the consistency limits, the liquid limit in particular, implies that a dispersed fabric dominates the clay–contaminant matrix (Mitchell and Soga 2005). As opposed to an edge–to–face flocculated fabric, a face–to–face aggregated (or dispersed) fabric offers less resistance to shear (or cone penetration), thereby leading to a decreased liquid limit. The location of the tested contaminated mixtures on Cassgrande's plasticity chart is illustrated in **Figures 1a** and **1b** for soils A and B, respectively. All soil A mixtures lie within the CI region (*clay with intermediate plasticity*) (see **Figure 1a**), while similar soil B mixtures position themselves within the CH region (*clay with high plasticity*) of the plasticity chart (see **Figure 1b**). The variations of *PI* against *LL* for both soil types followed a linear path. In this case, a conventional regression analysis indicated the existence of a rather strong linear agreement in the form of PI=0.49(LL+4.35) (with R^2=0.964) for soil A, and PI=0.55(LL+21.57) (with R^2=0.983) for soil B. For a given C_c, an increase in μ_c relocated both soil types towards lower plasticity regions. Similarly, for a given μ_c, an increase in C_c was accompanied by a similar yet slightly less pronounced relocation towards lower plasticity regions. In general, the magnitude of decrease in *LL* and *PI* was observed to be more significant for the soil of higher plasticity or soil B.

Typical stress–strain curves for the natural soil and various ethanol–contaminated samples are provided in **Figures 2a** and **2b** for soils A and B, respectively. A review of the stress–strain relationship indicated a rather strong inverse relationship between degree of contamination C_c and both the strength q_u and stiffness E of the contaminated soil, meaning that the greater the degree of contamination the greater the decrease in q_u and E (see the strength paths in **Figure 2**). On the contrary, an increase in C_c promoted a noticeable improvement in ε_u, thus avoiding brittle sample failure (see the strength paths in **Figure 2**). Maximum reduction in q_u and E was

observed in the case of C_c=8% ethanol inclusion. In this case, q_u and E dropped from 426.82 kPa and 30.06 MPa (corresponding to ε_u=2.6%) to 236.27 kPa and 11.04 MPa (corresponding to ε_u=3.4%) for soil A, respectively. For soil B, however, the magnitude of reduction was slightly greater, and q_u and E dropped from 359.70 kPa and 16.35 MPa (corresponding to ε_u=3.3%) to 163.36 kPa and 4.21 MPa (corresponding to ε_u=4.3%), respectively.

Typical stress–strain curves for the natural soil and the samples contaminated with C_c=6% glycerol, ethanol and ethylene glycol are provided in **Figures 3a** and **3b** for soils A and B, respectively. An increase in μ_c adversely affected the stress–strain response, leading to a significant decrease in both q_u and E (see the strength paths in **Figure 3**). Regarding ε_u, however, a noticeable increasing trend was observed with increase in μ_c (see the strength paths in **Figure 3**). These results justify the significant role portrayed by pore–fluid viscosity in describing the stress–strain response of the contaminated soil. For a given degree of contamination, C_c=6% for instance, maximum reduction in q_u and E was consistently observed for glycerol–contaminated samples, which also corresponds to the highest absolute viscosity (i.e. μ_c=4.310 cP). In this case, q_u and E experienced a significant decrease of 176.30 kPa and 18.57 MPa (corresponding to a 1% increase in ε_u) for soil A, and 184.52 kPa and 11.86 MPa (corresponding to a 1.2% increase in ε_u) for soil B, respectively.

Figures 4 and **5** illustrate the variations of q_u, E and ε_u against C_c for soils A and B, respectively. For a given type of soil, either soil A or B, the variations of q_u can be considered as a function of μ_c and C_c (see **Figures 4a** and **5a**). At a constant degree of contamination, an increase in μ_c leads to a significant decrease in q_u. Similarly, for a given μ_c, an increase in C_c is accompanied by a considerable yet less pronounced decrease in q_u. A review of **Figures 4b** and **5b** suggests a similar dependency for E. An opposite effect, however, can be concluded for ε_u, where an increase in either μ_c or C_c promotes a noticeable improvement in ε_u (see **Figures 4c** and

5c). Minimum reduction in q_u and E (corresponding to a minimum increase in ε_u) was observed for the samples contaminated with C_c=2% ethylene glycol (i.e. μ_c=1.181 cP). In this case, q_u and E exhibited a rather small decrease of 7.44 kPa and 2.83 MPa (corresponding to no increase in ε_u) for soil A, respectively. The magnitude of reduction for soil B was slightly more pronounced, where q_u and E experienced a decrease of 19.71 kPa and 2.64 MPa (corresponding to no increase in ε_u), respectively. The inclusion of C_c=8% glycerol (i.e. μ_c=4.310 cP) resulted in the lowest q_u and E (corresponding to the highest ε_u). In this case, q_u and E dropped from 426.82 kPa and 30.06 MPa (corresponding to ε_u=2.6%) to 206.09 kPa and 8.38 MPa (corresponding to ε_u=3.7%) for soil A, respectively. For soil B, a more apparent reduction can be observed, where q_u and E dropped from 359.70 kPa and 16.35 MPa (corresponding to ε_u=3.3%) to 130.98 kPa and 2.78 MPa (corresponding to ε_u=4.8%), respectively.

The test results are largely consistent with the majority of reported results found in the more recent literature sources (e.g. Ratnaweera and Meegoda 2006; Khamehchiyan et al. 2007; Estabragh et al. 2016b, 2016c; Nasehi et al. 2016; Estabragh et al. 2017). Any inconsistency can be attributed to the differences between the type of soil, the type of contaminant agent, and the range of tested degrees of contamination. The stress–strain response of a clay soil in the face of a varying pore–fluid composition is mainly governed by the net result of two different opposing or non–opposing mechanisms, i.e. physico–chemical interactions and mechanical factors (Ratnaweera and Meegoda 2006; Dolinar and Trauner 2007; Zhan et al. 2008; Olgun and Yıldız 2010; Liu et al. 2015; Estabragh et al. 2016b, 2016c, 2017). The physico–chemical effects are commonly interpreted by means of the diffuse double layer concept, which has been well–documented in the literature. Mechanical factors are mainly attributed to the pore–fluid viscosity, which in comparison has been less regarded in the literature.

In natural conditions, the pore–fluid of a clay soil contains a wide range of dissolved salts or cations and anions. A group of these cations are tightly attached to the clay surface, which neutralize the electrical charge on the clay surface. The excessive cations and anions are present as salt precipitates. With the addition of water, the precipitated salts go into solution. Desorption of cations from the clay surface leads to a higher concentration of cations near the clay surface, which in turn promotes a tendency among cations to diffuse away. This tendency for diffusion, however, is restricted by the attractive forces present between the cations and the surface of the negatively charged clay particle. The outcome of these opposing actions promotes the development of an ion distribution in the vicinity of the clay particle. The negatively charged surface of the clay particle, along with the distributed ions in the adjacent phase, is referred to as the diffuse double layer or DDL (Mitchell and Soga 2005). The DDL can develop for individual clay particles. These individually developed DDLs can interact with each other. This can lead to a change in thickness of the DDL, which is accompanied by a net repulsive or attractive force between two clay particles. Changes in thickness of the DDL results in different fabric of soil, and thus different mechanical behavior. Thickness of the DDL is often interpreted in accordance with the Gouy and Chapman theory, which can be expressed by the following relationship developed by Mitchell and Soga (2005):

$$\frac{1}{k} = \sqrt{\frac{\varepsilon_0 DKT}{2\eta_0 e^2 v^2}} \tag{1}$$

where $1/k$=equivalent thickness of the DDL (in Å); ε_0=permittivity of vacuum (=8.8542×10^{-12} $C^2J^{-1}m^{-1}$); D=dielectric constant of the pore–fluid; K=Boltzmann constant (=1.38×10^{-23} J^oK^{-1}); T=absolute temperature (in ^oK); η_0=pore–fluid concentration (in ions/m^3); e=electronic charge (=1.602×10^{23} C); and v=cation valence.

Based on Equation (1), thickness of the DDL is proportional to the square root of the pore–fluid's dielectric constant. Therefore, any noticeable decrease in the pore–fluid's dielectric constant is expected to decrease the DDL thickness, and thus promote a flocculated soil fabric (owing to the presence of a dominant net attractive van der Waals force) accompanied by an improvement in strength characteristics (Sridharan and Venkatappa Rao 1973; Moore and Mitchell 1974; Sridharan and Venkatappa Rao 1979; Anandarajah and Zhao 2000; Olgun and Yıldız 2010; Khosravi et al. 2013; Estabragh et al. 2016a). As demonstrated in **Table 3**, however, $D^{0.5}$ for the used contaminant agents is approximately equal to that of deionized water (i.e. $D^{0.5}$=8.86). Therefore, the stress–strain response can be considered as independent from the physico–chemical effects, and thus strongly dominated by mechanical factors such as pore–fluid viscosity. In general, an increase in pore–fluid viscosity, as the case with the used contaminant agents in this study (see **Table 3**), facilitates sliding of particles during unconfined loading due to lubrication of soil particles. This in turn promotes a reduced friction among particles, which is accompanied by a decreased strength and stiffness often coupled with an improved ductility (Meegoda and Ratnaweera 1994; Ratnaweera and Meegoda 2006; Khamehchiyan et al. 2007; Singh et al. 2008; Liu et al. 2015; Estabragh et al. 2016b, 2016c; Nasehi et al. 2016; Estabragh et al. 2017; Soltani et al. 2017a).

Dimensional analysis

Model development

The derivation of a dimensional model accounting for all variables governing a physical problem, the shear strength phenomenon in this case, is a formidable task. A practical dimensional model can be characterized as one that maintains a perfect balance between simplicity (ease of application) and accuracy, thus involving a limited number of conventional physical parameters capable of arriving at a reliable estimate of the problem in hand. It is

therefore essential avoiding the introduction of any physical parameters which are equally (or more) difficult to measure compared with the physical problem intended to be modeled. For a given type of soil exposed to a viscous–dominant contaminant agent, the variables governing the unconfined compressive strength q_u can be categorized into three groups, each representing a component of the soil–water–contaminant system. The three groups and their respective variables can be given as:

- **Soil:** W_s=weight; γ_{d0}= initial dry unit weight; and SSA=specific surface area.
- **Water:** W_w=weight; and μ_w=absolute viscosity.
- **Contaminant:** W_c=weight; and μ_c=absolute viscosity.

Therefore, one can represent q_u by the following functional expression:

$$q_u = f(\underbrace{W_s, \gamma_{d0}, SSA}_{\text{Soil}}, \overbrace{W_w, \mu_w}^{\text{Water}}, \underbrace{W_c, \mu_c}_{\text{Contaminant}}) \tag{2}$$

where f=an unknown multi–variable function.

The empirical relationship developed by Locat et al. (1984) can be employed to obtain the specific surface area of the contaminated soil by means of the plasticity index:

$$SSA = \frac{PI}{0.7} + 5 \tag{3}$$

where SSA=specific surface area (in m^2/gr); and PI=plasticity index (in %, as provided in **Table 4**).

Although the shear strength of an unsaturated geomaterial, such as the contaminated soil in this study, is well–known to be related to its matric suction, one may argue that an accurate measurement of suction, for fine–grained soils in particular, is a rather difficult and time–consuming task (Johari et al. 2006; Agus et al. 2010; Malaya and Sreedeep 2011). A typical unconfined compression test (the problem in hand), however, is deemed as a routine test commonly performed in most laboratories with much less effort. To maintain model

simplicity/practicality, it was therefore decided to disregard introducing suction as a governing variable. Such a simplification also complies with most of the existing literature, where various forms of empirical and dimensional models have been developed (and validated) for different geomaterials without regarding suction as an input variable (e.g. Rao et al. 2004; Buzzi et al. 2011; Williamson and Cortes 2014; Berrah et al. 2016; Zhao et al. 2016).

The Buckingham π theorem provides a method for computing sets of dimensionless parameters from given variables, even if the form of the equation remains unknown (Buckingham 1914). The concept is recognized as a well–established rule in fluid mechanics, while it has been less regarded in geotechnical–related disciplines (e.g. Butterfield 1999; Buzzi 2010; Buzzi et al. 2011; Williamson and Cortes 2014; Berrah et al. 2016; Zhao et al. 2016). In accordance with the Buckingham concept, the system of 7 independent variables (γ_{d0} is related to W_s) and 3 dimensions (i.e. mass [M], length [L] and time [T]) given in Equation (2) can be further reduced to 7–3=4 dimensionless parameters, referred to as π terms, which can be given as:

$$\pi_0 = \frac{q_u}{\mu_w \sqrt{\gamma_{d0} SSA}} \tag{4}$$

$$\pi_1 = \frac{W_c}{W_s} = C_c \tag{5}$$

$$\pi_2 = \frac{W_w}{W_s} = \omega_0 \tag{6}$$

$$\pi_3 = \frac{\mu_c}{\mu_w} \tag{7}$$

The variations of π_0 (i.e. the dependent π term) against π_1, π_2 and π_3 (i.e. the independent π terms) were plotted over an arithmetic plot, as shown in **Figure 6**. The three independent π terms seem to strongly influence π_0, and thus hold physical significance for model development.

Through trial and error, a new dimensionless parameter (denoted as the dimensionless viscosity number μ^*) was obtained, which can be given as:

$$\mu^* = \frac{\pi_1 \pi_3}{\pi_2} = \frac{C_c \mu_c}{\omega_0 \mu_w} \tag{8}$$

where for the natural soil (i.e. water as the pore–fluid) $\mu^*=0$.

It should be noted that the initial moisture content of the soil–water–contaminant mixture (i.e. ω'_0 which is equal to the optimum moisture content ω'_{opt}, as provided in **Table 4**) was defined as the addition of the initial water content, i.e. $\omega_0=W_w/W_s$, and the degree of contamination, i.e. $C_c=W_c/W_s$. The variations of π_0 against the newly introduced dimensionless parameter μ^* were plotted for both soils A and B over an arithmetic space, as shown in **Figure 7a**. A review of the π_0–μ^* plot indicated the existence of a rather strong relationship in the form of a conventional three–parameter exponential function between π_0 and μ^*. Therefore, one can conclude the following:

$$\pi_0 = \alpha_0 + \alpha_1 \exp(\alpha_2 \mu^*) \tag{9}$$

where α_0, α_1 and α_2=fitting parameters.

By equating Equations (4) and (9) and rearranging, the following can be derived for q_u:

$$q_u = \mu_w \sqrt{\gamma_{d0} SSA} \left[\alpha_0 + \alpha_1 \exp(\alpha_2 \mu^*)\right] \tag{10}$$

An attempt was made to extend the aforementioned concept proposed for q_u to the modulus of elasticity E. In this case, the π_0–μ^* plot corresponding to E data also exhibited an exponential trend similar to that of observed for q_u (see **Figure 7b**). Therefore, one can conclude the following for E:

$$E = \mu_w \sqrt{\gamma_{d0} SSA} \left[\beta_0 + \beta_1 \exp(\beta_2 \mu^*)\right] \tag{11}$$

where β_0, β_1 and β_2=fitting parameters.

The fitting parameters α_0 to α_2 and β_0 to β_2 were obtained by means of the non–linear least squares optimization technique. Statistical fit–measure indices, i.e. the coefficient of determination R^2, the root mean squares error RMSE (in kPa), the normalized root mean squares error NRMSE (in %), and the mean absolute percentage error MAPE (in %), were obtained for model validation by the following relationships:

$$\mathrm{RMSE} = \sqrt{\frac{1}{n}\sum_{j=1}^{n}(y_{mj} - y_{aj})^2} \tag{12}$$

$$\mathrm{NRMSE} = \frac{\mathrm{RMSE}}{y_{a\max} - y_{a\min}} \times 100 \tag{13}$$

$$\mathrm{MAPE} = \frac{1}{n}\sum_{j=1}^{n}\left|\frac{y_{mj} - y_{aj}}{y_{aj}}\right| \times 100 \tag{14}$$

where y_m=predicted value of the dependent variable y (=q_u or E); y_a=actual value of the dependent variable y; $y_{a\max}$=maximum value of y_a data; $y_{a\min}$=minimum value of y_a data; j=index of summation; and n=number of data points used for model development (=13 for each soil).

Sensitivity analysis

In order to quantify the influence of the contaminant properties, i.e. μ_c and C_c, on the strength characteristics, i.e. q_u and E, a sensitivity analysis was carried out. Since q_u and E are currently defined as continuous mathematical functions, i.e. Equations (10) and (11), the partial derivative sensitivity analysis technique may be the most suitable approach (Estabragh et al. 2016d; Soltani 2017; Soltani et al. 2017c, 2018b). For this purpose, Equations (10) and (11) were first revised in accordance with the definition of μ^* to obtain relationships which are directly defined as a function of μ_c and C_c. In this case, the following can be obtained for q_u and E, respectively:

$$q_u = \mu_w \sqrt{\gamma_{d0} SSA}\left[\alpha_0 + \alpha_1 \exp\left(\frac{\alpha_2 C_c \mu_c}{\omega_0 \mu_w}\right)\right] \tag{15}$$

$$E = \mu_w \sqrt{\gamma_{d0} SSA}\left[\beta_0 + \beta_1 \exp\left(\frac{\beta_2 C_c \mu_c}{\omega_0 \mu_w}\right)\right] \quad (16)$$

Assuming μ_c and C_c as x_i, the relative impact of the independent variable x_i on the dependent variable y (=q_u or E), referred to as sensitivity or $S(x_i)$, can be defined as:

$$S(x_i) = \frac{\sigma(x_i)}{n\sigma(y)} \sum_{j=1}^{n} \left|\frac{\partial y}{\partial x_i}\right|_j \quad 17)$$

where $\partial y/\partial x_i$=partial derivative of y (=q_u or E) with respect to x_i (=μ_c and C_c); $\sigma(y)$=standard deviation of predicted y data; and $\sigma(x_i)$=standard deviation of x_i data.

The partial derivative $\partial y/\partial x_i$ with respect to x_i=μ_c and C_c can be expressed by the following:

$$\frac{\partial q_u}{\partial \mu_c} = \frac{\alpha_1 \alpha_2 C_c \sqrt{\gamma_{d0} SSA}}{\omega_0} \exp\left(\frac{\alpha_2 C_c \mu_c}{\omega_0 \mu_w}\right) \quad (18)$$

$$\frac{\partial q_u}{\partial C_c} = \frac{\alpha_1 \alpha_2 \mu_c \sqrt{\gamma_{d0} SSA}}{\omega_0} \exp\left(\frac{\alpha_2 C_c \mu_c}{\omega_0 \mu_w}\right) \quad (19)$$

$$\frac{\partial E}{\partial \mu_c} = \frac{\beta_1 \beta_2 C_c \sqrt{\gamma_{d0} SSA}}{\omega_0} \exp\left(\frac{\beta_2 C_c \mu_c}{\omega_0 \mu_w}\right) \quad (20)$$

$$\frac{\partial E}{\partial C_c} = \frac{\beta_1 \beta_2 \mu_c \sqrt{\gamma_{d0} SSA}}{\omega_0} \exp\left(\frac{\beta_2 C_c \mu_c}{\omega_0 \mu_w}\right) \quad (21)$$

The partial derivative term $\partial y/\partial x_i$ represents the likelihood of y increasing or decreasing as a result of increase in x_i. Therefore, the likelihood of increase, i.e. $P(x_i)^+$, or decrease, i.e. $P(x_i)^-$, in y as a result of increase in x_i can be given as:

$$P(x_i)^+ = \frac{m(x_i)^+}{n} \times 100 \quad (22)$$

$$P(x_i)^- = \frac{m(x_i)^-}{n} \times 100 \quad (23)$$

where $m(x_i)^+$=number of observations where $\partial y/\partial x_i>0$; and $m(x_i)^-$=number of observations where $\partial y/\partial x_i<0$.

The positive, i.e. $\eta(x_i)^+$, and negative, i.e. $\eta(x_i)^-$, magnitudes on y caused by increase in x_i can be defined as:

$$\eta(x_i)^+ = \frac{\sigma(x_i)}{n\sigma(y)} \sum_{j=1}^{n} \left| \frac{\partial y}{\partial x_i} \right|_j \; ; \; \forall x_i \ni \frac{\partial y}{\partial x_i} > 0 \tag{24}$$

$$\eta(x_i)^- = \frac{\sigma(x_i)}{n\sigma(y)} \sum_{j=1}^{n} \left| \frac{\partial y}{\partial x_i} \right|_j \; ; \; \forall x_i \ni \frac{\partial y}{\partial x_i} < 0 \tag{25}$$

where the positive and negative magnitudes resemble positive and negative fractions of the sensitivity parameter $S(x_i)$, meaning that for a given x_i, $S(x_i)=\eta(x_i)^+ + \eta(x_i)^-$.

Discussion of model prediction

The regression analysis outputs with respect to the proposed dimensional models for q_u and E, i.e. Equations (10) and (11), are summarized in **Table 5**. The proposed relationships well correlate with experimental data. The high R^2 and low RMSE, NRMSE and MAPE values imply a high agreement between actual and predicted data, both in terms of correlation and error. The R^2 values were mainly above the 0.98 margin, meaning that approximately 98% of the variations in experimental observations are explained by the proposed relationships. The NRMSE and MAPE values were observed to be less than the 5% for majority of cases, indicating an average offset of 5% associated with the predictive capacity of the dimensional models. **Figures 8a** and **8b** illustrate actual versus predicted q_u and E data along with corresponding 95% confidence intervals, respectively. All data points fall between the upper and lower 95% confidence intervals, indicating no particular outliners associated with the predictions. The R^2 was also obtained for these combined datasets, which resulted in a net R^2 of 0.981 and 0.994 for q_u and E, respectively. It should be noted that the proposed dimensional models given in Equations (10) and (11) were developed based on two tested soils. Moreover, the equations are only valid when

soils are compacted at Proctor optimum condition, which is often implemented in the field. Additional testing at dry of optimum and wet of optimum conditions should be carried out to arrive at generalized equations capable of quantifying the stress–strain response of the contaminated soil at varying initial placement conditions. The proposed dimensional models each contain a total of three model (or fitting) parameters. The model parameters can be adequately estimated by a total of three unconfined compression tests. For a given soil type, three scenarios consisting of the natural soil and two contaminated samples are suggested for the calibration phase. The choice of contaminant viscosity and degree of contamination for the two contaminated samples would be arbitrary. From a statistical perspective, however, a high and low viscosity both corresponding to a median degree of contamination is expected to yield a more reliable estimate of the model parameters (Mirzababaei et al. 2018).

The sensitivity analysis results for μ_c and C_c with respect to the proposed dimensional models are summarized in **Table 6**. A review of the sensitivity parameter $S(x_i)$ indicates that the variations in both q_u and E are mainly controlled and dominated by μ_c. All $S(x_i)$ values for μ_c were observed to be greater than those determined for C_c ($S(\mu_c)>S(C_c)$). For q_u, $S(\mu_c)$ and $S(C_c)$ were observed to be 0.62 and 0.49 for soil A, respectively. For soil B, however, these values were slightly greater, and were obtained as $S(\mu_c)=0.65$ and $S(C_c)=0.53$. A similar case can also be made regarding E (i.e. $S(\mu_c)=0.66$ and $S(C_c)=0.54$ for soil A; and $S(\mu_c)=0.71$ and $S(C_c)=0.60$ for soil B). Such trends indicate that soil B (i.e. CH type) is more sensitive to the variations of μ_c and C_c, and thus contamination in general, compared to soil A (i.e. CI type). The likelihood of increase in q_u or E as a result of increase in μ_c and C_c was observed to be $P(x_i)^+=0$ for all cases, which strongly indicates the existence of an inverse relationship between q_u or E and μ_c and C_c. Therefore, the magnitude of decrease in q_u or E as a result of increase in μ_c and C_c suggested

equal values to that of $S(x_i)$, i.e. $S(x_i)=\eta(x_i)^{-}$, which essentially justifies the inverse relationship between q_u or E and μ_c and C_c.

Summary and conclusions

An experimental program was developed to investigate the influence of three viscous–dominant contaminants on the stress–strain response of two clay soils. The dimensional analysis concept was also implemented to the test results, thereby deriving a practical model capable of predicting the stress–strain response of contaminated soils. The following conclusions can be drawn from this study:

- Lubrication at particle contact level caused by the viscous nature of the contaminant agent portrayed a significant role in describing the stress–strain response of the contaminated soil. The stress–strain relationship was adversely affected by contamination. The strength properties q_u and E were observed to be inversely related to μ_c and C_c. At a constant C_c, an increase in μ_c led to a significant decrease in q_u and E, while a noticeable improvement in ε_u was observed. Similarly, for a given μ_c, an increase in C_c suggested a considerable yet less pronounced decrease in q_u and E.
- The dimensional analysis concept was successfully implemented to quantify the stress–strain response of the contaminated soil. A new dimensionless parameter, denoted as the dimensionless viscosity number μ^*, was introduced as the governing variable capable of describing the stress–strain behavior of the contaminated soil, i.e. q_u and $E=f(\mu^*)$. The predictive capacity of the proposed dimensional models was examined and further confirmed by statistical techniques. The proposed dimensional models contain a limited number of fitting parameters, which can be calibrated by minimal experimental effort, and thus can be useful for predictive purposes.

References

Abdul, A. S., Gibson, T. L. & Rai, D. N. (1990). Laboratory studies of the flow of some organic solvents and their aqueous solutions through bentonite and kaolin clays. *Ground Water* **28**, No. 4, 524–533, http://dx.doi.org/10.1111/j.1745-6584.1990.tb01708.x.

Agus, S. S., Schanz, T. & Fredlund, D. G. (2010). Measurements of suction versus water content for bentonite–sand mixtures. *Canadian Geotechnical Journal* **47**, No.5, 583–594, http://dx.doi.org/10.1139/t09-120.

Al-Rawas, A., Hassan, H. F., Taha, R., Hago, A., Al-Shandoudi, B. & Al-Suleimani, Y. (2005). Stabilization of oil–contaminated soils using cement and cement by–pass dust. *Management of Environmental Quality: An International Journal* **16**, No. 6, 670–680, http://dx.doi.org/10.1108/14777830510623736.

Al-Sanad, H. A., Eid, W. K. & Ismael, N. F. (1995). Geotechnical properties of oil–contaminated Kuwaiti sand. *Journal of Geotechnical Engineering* **121**, No. 5, 407–412, http://dx.doi.org/10.1061/(asce)0733-9410(1995)121:5(407).

Anandarajah, A. & Zhao, D. (2000). Triaxial behavior of kaolinite in different pore fluids. *Journal of Geotechnical and Geoenvironmental Engineering* **126**, No. 2, 148–156, http://dx.doi.org/10.1061/(asce)1090-0241(2000)126:2(148).

Benson, C. H., Meegoda, J. N., Gilbert, R. B. & Clemence, S. P. (1998). Geotechnical special publication No. 82: Risk–based corrective action and brownfields restorations. ASCE, New York: NY, http://dx.doi.org/10.1061/9780784403891.

Berrah, Y., Boumezbeur, A., Kherici, N. & Charef, N. (2016). Application of dimensional analysis and regression tools to estimate swell pressure of expansive soil in Tebessa (Algeria). *Bulletin of Engineering Geology and the Environment* **in press**, http://dx.doi.org/10.1007/s10064-016-0973-4.

Bowders Jr., J. J. & Daniel, D. E. (1987). Hydraulic conductivity of compacted clay to dilute organic chemicals. *Journal of Geotechnical Engineering* **113**, No. 12, 1432–1448, http://dx.doi.org/10.1061/(asce)0733-9410(1987)113:12(1432).

Buckingham, E. (1914). On physically similar systems; illustrations of the use of dimensional equations. *Physical Review* **4**, No. 4, 345–376, http://dx.doi.org/10.1103/physrev.4.345.

Butterfield, R. (1999). Dimensional analysis for geotechnical engineers. *Géotechnique* **49**, No. 3, 357–366, http://dx.doi.org/10.1680/geot.1999.49.3.357.

Buzzi, O. (2010). On the use of dimensional analysis to predict swelling strain. *Engineering Geology* **116**, No. 1–2, 149–156, http://dx.doi.org/10.1016/j.enggeo.2010.08.005.

Buzzi, O., Giacomini, A. & Fityus, S. (2011). Towards a dimensionless description of soil swelling behaviour. *Géotechnique* **61**, No. 3, 271–277, http://dx.doi.org/10.1680/geot.7.00194.

Chen, J., Anandarajah, A. & Inyang, H. (2000). Pore fluid properties and compressibility of kaolinite. *Journal of Geotechnical and Geoenvironmental Engineering* **126**, No. 9, 798–807, http://dx.doi.org/10.1061/(asce)1090-0241(2000)126:9(798).

Di Matteo, L., Bigotti, F. & Ricco, R. (2011). Compressibility of kaolinitic clay contaminated by ethanol–gasoline blends. *Journal of Geotechnical and Geoenvironmental Engineering* **137**, No. 9, 846–849, http://dx.doi.org/10.1061/(asce)gt.1943-5606.0000494.

Dolinar, B. & Trauner, L. (2007). The impact of structure on the undrained shear strength of cohesive soils. *Engineering Geology* **92**, No. 1–2, 88–96, http://dx.doi.org/10.1016/j.enggeo.2007.04.003.

Estabragh, A. R., Beytolahpour, I., Moradi, M. & Javadi, A. A. (2014). Consolidation behavior of two fine–grained soils contaminated by glycerol and ethanol. *Engineering Geology* **178**, 102–108, http://dx.doi.org/10.1016/j.enggeo.2014.05.017.

Estabragh, A. R., Beytolahpour, I., Moradi, M. & Javadi, A. A. (2016a). Mechanical behavior of a clay soil contaminated with glycerol and ethanol. *European Journal of Environmental and Civil Engineering* **20**, No. 5, 503–519, http://dx.doi.org/10.1080/19648189.2015.1047900.

Estabragh, A. R., Khatibi, M. & Javadi, A. A. (2016b). Effect of cement on treatment of a clay Soil contaminated with glycerol. *Journal of Materials in Civil Engineering* **28**, No. 4, 4015157-1–4015157-10, http://dx.doi.org/10.1061/(asce)mt.1943-5533.0001443.

Estabragh, A. R., Khatibi, M. & Javadi, A. A. (2016c). Effect of cement on mechanical behavior of soil contaminated with monoethylene glycol (MEG). *ACI Materials Journal* **113**, No. 6, 709–717, http://dx.doi.org/10.14359/51689236.

Estabragh, A. R., Kholoosi, M. M., Ghaziani, F. & Javadi, A. A. (2017). Stabilization and solidification of a clay soil contaminated with MTBE. *Journal of Environmental Engineering* **143**, No. 9, 4017054-1–4017054-8, http://dx.doi.org/10.1061/(asce)ee.1943-7870.0001248.

Estabragh, A. R., Soltani, A. & Javadi, A. A. (2016d). Models for predicting the seepage velocity and seepage force in a fiber reinforced silty soil. *Computers and Geotechnics* **75**, 174–181, http://dx.doi.org/10.1016/j.compgeo.2016.02.002.

Fang, H. (1997). Nature of soil and environment. In *Introduction to environmental geotechnology* (1st ed). CRC Press, Boca Raton: FL, pp. 49–78.

Fatahi, B., Khabbaz, H. & Fatahi, B. (2012). Mechanical characteristics of soft clay treated with fibre and cement. *Geosynthetics International* **19**, No. 3, 252–262, http://dx.doi.org/10.1680/gein.12.00012.

Fernandez, F. & Quigley, R. M. (1985). Hydraulic conductivity of natural clays permeated with simple liquid hydrocarbons. *Canadian Geotechnical Journal* **22**, No. 2, 205–214, http://dx.doi.org/10.1139/t85-028.

Hassan, H. F., Taha, R., Al-Rawas, A., Al-Shandoudi, B., Al-Gheithi, K. & Al-Barami, A. M. (2005). Potential uses of petroleum–contaminated soil in highway construction. *Construction and Building Materials* **19**, No. 8, 646–652, http://dx.doi.org/10.1016/j.conbuildmat.2005.01.001.

Johari, A., Habibagahi, G. & Ghahramani, A. (2006). Prediction of soil–water characteristic curve using genetic programming. *Journal of Geotechnical and Geoenvironmental Engineering* **132**, No.5, 661–665, http://dx.doi.org/10.1061/(asce)1090-0241(2006)132: 5(661).

Kaya, A. & Fang, H. (2000). The effects of organic fluids on physicochemical parameters of fine–grained soils. *Canadian Geotechnical Journal* **37**, No. 5, 943–950, http://dx.doi.org/10.1139/t00-023.

Kermani, M. & Ebadi, T. (2012). The effect of oil contamination on the geotechnical properties of fine–grained soils. *Soil and Sediment Contamination* **21**, No. 5, 655–671, http://dx.doi.org/10.1080/15320383.2012.672486.

Khamehchiyan, M., Charkhabi, A. H. & Tajik, M. (2007). Effects of crude oil contamination on geotechnical properties of clayey and sandy soils. *Engineering Geology* **89**, No. 3–4, 220–229, http://dx.doi.org/10.1016/j.enggeo.2006.10.009.

Khosravi, E., Ghasemzadeh, H., Sabour, M. R. & Yazdani, H. (2013). Geotechnical properties of gas oil–contaminated kaolinite. *Engineering Geology* **166**, 11–16, http://dx.doi.org/10.1016/j.enggeo.2013.08.004.

Kim, S. & Palomino, A. M. (2009). Polyacrylamide–treated kaolin: A fabric study. *Applied Clay Science* **45**, No.4, 270–279, http://dx.doi.org/10.1016/j.clay.2009.06.009.

Kjeldsen, P., Barlaz, M. A., Rooker, A. P., Baun, A., Ledin, A. & Christensen, T. H. (2002). Present and long–term composition of MSW landfill leachate: A review. *Critical Reviews in Environmental Science and Technology* **32**, No. 4, 297–336, http://dx.doi.org/10.1080/10643380290813462.

Liu, Z., Liu, S. & Cai, Y. (2015). Engineering property test of kaolin clay contaminated by diesel oil. *Journal of Central South University* **22**, No. 12, 4837–4843, http://dx.doi.org/10.1007/s11771-015-3035-3.

Locat, J., Lefebvre, G. & Ballivy, G. (1984). Mineralogy, chemistry, and physical properties interrelationships of some sensitive clays from Eastern Canada. *Canadian Geotechnical Journal* **21**, No. 3, 530–540, http://dx.doi.org/10.1139/t84-055.

Malaya, C. & Sreedeep, S. (2011). A Laboratory Procedure for Measuring High Soil Suction. *Geotechnical Testing Journal* **34**, No.5, 396–405, http://dx.doi.org/10.1520/gtj103613.

Meegoda, J. N. & Ratnaweera, P. (2008). Prediction of effective porosity of contaminated fine grained soils using electrical properties. *Geotechnical Testing Journal* **31**, No. 4, 344–357, http://dx.doi.org/10.1520/gtj100969.

Meegoda, J. N., Chen, B., Gunasekera, S. D. & Pederson, P. (1998). Compaction characteristics of contaminated soils–reuse as a road base material. In *Geotechnical special publication No. 79: Recycled materials in geotechnical applications* (Vipulanandan, C. & Elton, D. J. eds). ASCE, Boston: MA, pp. 195–209.

Meegoda, J. N., Vallejo, L. E. & Reddi, L. N. (1996). Geotechnical special publication No. 59: Engineered contaminated soils and interaction of soil geomembranes. ASCE, New York: NY.

Meegoda, N. J. & Gunasekera, S. D. (1992). A new method to measure the effective porosity of clays. *Geotechnical Testing Journal* **15**, No. 4, 340–351, http://dx.doi.org/10.1520/gtj10248j.

Meegoda, N. J. & Rajapakse, R. A. (1993). Short–term and long–term permeabilities of contaminated clays. *Journal of Environmental Engineering* **119**, No. 4, 725–743, http://dx.doi.org/10.1061/(asce)0733-9372(1993)119:4(725).

Meegoda, N. J. & Ratnaweera, P. (1994). Compressibility of contaminated fine–grained soils. *Geotechnical Testing Journal* **17**, No. 1, 101–112, http://dx.doi.org/10.1520/gtj10078j.

Meegoda, N. J. & Ratnaweera, P. (1995). Treatment of oil–contaminated soils for identification and classification. *Geotechnical Testing Journal* **18**, No. 1, 41–49, http://dx.doi.org/10.1520/gtj10120j.

Mesri, G. & Olson, R. E. (1971). Mechanisms controlling the permeability of clays. *Clays and Clay Minerals* **19**, No. 3, 151–158, http://dx.doi.org/10.1346/ccmn.1971.0190303.

Michaels, A. S. & Lin, C. S. (1954). Permeability of kaolinite. *Industrial and Engineering Chemistry* **46**, No. 6, 1239–1246, http://dx.doi.org/10.1021/ie50534a041.

Mirzababaei, M., Mohamed, M., Arulrajah, A., Horpibulsuk, S. & Anggraini, V. (2018). Practical approach to predict the shear strength of fibre–reinforced clay. *Geosynthetics International* **25**, No. 1, 50–66, http://dx.doi.org/10.1680/jgein.17.00033.

Mitchell, J. K. & Soga, K. (2005). Soil–water–chemical interactions. In *Fundamentals of soil behavior* (3rd ed). John Wiley & Sons, Hoboken: NJ, pp. 143–172, http://dx.doi.org/10.2136/sssaj1976.03615995004000040003x.

Moavenian, M. H. & Yasrobi, S. S. (2008). Volume change behavior of compacted clay due to organic liquids as permeant. *Applied Clay Science* **39**, No. 1–2, 60–71, http://dx.doi.org/10.1016/j.clay.2007.04.009.

Moore, C. A. & Mitchell, J. K. (1974). Electromagnetic forces and soil strength. *Géotechnique* **24**, No. 4, 627–640, http://dx.doi.org/10.1680/geot.1974.24.4.627.

Nasehi, S. A., Uromeihy, A., Nikudel, M. R. & Morsali, A. (2016). Influence of gas oil contamination on geotechnical properties of fine and coarse–grained soils. *Geotechnical and Geological Engineering* **34**, No. 1, 333–345, http://dx.doi.org/10.1007/s10706-015-9948-7.

Olgun, M. & Yıldız, M. (2010). Effect of organic fluids on the geotechnical behavior of a highly plastic clayey soil. *Applied Clay Science* **48**, No. 4, 615–621, http://dx.doi.org/10.1016/j.clay.2010.03.015.

Park, J., Vipulanandan, C., Kim, J. W. & Oh, M. H. (2006). Effects of surfactants and electrolyte solutions on the properties of soil. *Environmental Geology* **49**, No.7, 977–989, http://dx.doi.org/10.1007/s00254-005-0136-6.

Rao, A. S., Phanikumar, B. R. & Sharma, R. S. (2004). Prediction of swelling characteristics of remoulded and compacted expansive soils using free swell index. *Quarterly Journal of Engineering Geology and Hydrogeology* **37**, No.3, 217–226, http://dx.doi.org/10.1144/1470-9236/03-052.

Rao, S. M. & Sridharan, A. (1985). Mechanism controlling the volume change behavior of kaolinite. *Clays and Clay Minerals* **33**, No. 4, 323–328, http://dx.doi.org/10.1346/ccmn.1985.0330407.

Ratnaweera, P. & Meegoda, J. N. (2006). Shear strength and stress–strain behavior of contaminated soils. *Geotechnical Testing Journal* **29**, No. 2, 1–8, http://dx.doi.org/10.1520/gtj12686.

Singh, S. K., Srivastava, R. K. & John, S. (2008). Settlement characteristics of clayey soils contaminated with petroleum hydrocarbons. *Soil and Sediment Contamination* **17**, No. 3, 290–300, http://dx.doi.org/10.1080/15320380802007028.

Soltani, A. (2017). Discussion of "Optimization of carpet waste fibers and steel slag particles to reinforce expansive soil using response surface methodology" by M. Shahbazi, M. Rowshanzamir, S.M. Abtahi, S.M. Hejazi [Appl. Clay Sci., doi:10.1016/j.clay.2016.11.027]. *Applied Clay Science* **in press**, http://dx.doi.org/10.1016/j.clay.2017.07.020.

Soltani, A., Azimi, M., Deng, A. & Taheri, A. (2017c). A simplified method for determination of the soil–water characteristic curve variables. *International Journal of Geotechnical Engineering* **in press**, http://dx.doi.org/10.1080/19386362.2017.1344450.

Soltani, A., Deng, A., Taheri, A. & Mirzababaei, M. (2017a). A sulphonated oil for stabilisation of expansive soils. *International Journal of Pavement Engineering* **in press**, http://dx.doi.org/10.1080/10298436.2017.1408270.

Soltani, A., Deng, A., Taheri, A. & Mirzababaei, M. (2018a). Rubber powder–polymer combined stabilization of South Australian expansive soils. *Geosynthetics International* **in press**, http://dx.doi.org/10.1680/jgein.18.00009.

Soltani, A., Deng, A., Taheri, A., Sridharan, A. & Estabragh, A. R. (2018b). A framework for interpretation of the compressibility behavior of soils. *Geotechnical Testing Journal* **41**, No. 1, http://dx.doi.org/10.1520/GTJ20170088.

Soltani, A., Taheri, A., Khatibi, M. & Estabragh, A. R. (2017b). Swelling potential of a stabilized expansive soil: A comparative experimental study. *Geotechnical and Geological Engineering* **35**, No. 4, 1717–1744, http://dx.doi.org/10.1007/s10706-017-0204-1.

Sridharan, A. & Prakash, K. (1999). Mechanisms controlling the undrained shear strength behaviour of clays. *Canadian Geotechnical Journal* **36**, No. 6, 1030–1038, http://dx.doi.org/10.1139/t99-071.

Sridharan, A. & Venkatappa Rao, G. (1973). Mechanisms controlling volume change of saturated clays and the role of the effective stress concept. *Géotechnique* **23**, No. 3, 359–382, http://dx.doi.org/10.1680/geot.1973.23.3.359.

Sridharan, A. & Venkatappa Rao, G. (1979). Shear strength behaviour of saturated clays and the role of the effective stress concept. *Géotechnique* **29**, No. 2, 177–193, http://dx.doi.org/10.1680/geot.1979.29.2.177.

Tremblay, H., Duchesne, J., Locat, J. & Leroueil, S. (2002). Influence of the nature of organic compounds on fine soil stabilization with cement. *Canadian Geotechnical Journal* **39**, No. 3, 535–546, http://dx.doi.org/10.1139/t02-002.

Tuncan, A., Tuncan, M. & Koyuncu, H. (2000). Use of petroleum–contaminated drilling wastes as sub–base material for road construction. *Waste Management and Research* **18**, No. 5, 489–505, http://dx.doi.org/10.1177/0734242x0001800511.

Williamson, S. & Cortes, D. D. (2014). Dimensional analysis of soil–cement mixture performance. *Géotechnique Letters* **4**, No.1, 33–38, http://dx.doi.org/10.1680/geolett.13.00082.

Wroth, C. P. & Wood, D. M. (1978). The correlation of index properties with some basic engineering properties of soils. *Canadian Geotechnical Journal* **15**, No.2, 137–145, http://dx.doi.org/10.1139/t78-014.

Zhan, T. L. T., Chen, Y. M. & Ling, W. A. (2008). Shear strength characterization of municipal solid waste at the Suzhou landfill, China. *Engineering Geology* **97**, No. 3–4, 97–111, http://dx.doi.org/10.1016/j.enggeo.2007.11.006.

Zhao, Y., Gao, Y., Zhang, Y. & Wang, Y. (2016). Effect of fines on the mechanical properties of composite soil stabilizer–stabilized gravel soil. *Construction and Building Materials* **126**, 701–710, http://dx.doi.org/10.1016/j.conbuildmat.2016.09.082

Accepted manuscript
doi: 10.1680/jenge.18.00018

Table 1. A summary of the studies on soil contamination

Reference	Soil(s)	Contaminant(s)	Highlights [1]
Meegoda and Ratnaweera (1994)	ML [2] CH [3]	Glycerol Propanol	▪ Increase in both the liquid limit and the compression index for the ML soil contaminated with propanol (no significant variation nor trend was observed for the CH soil contaminated with glycerol) ▪ Decrease in the plastic limit
Al-Sanad et al. (1995)	SP [4]	Benzene Crude oil Gas oil	▪ Increase in the maximum dry unit weight (expect for high oil inclusions), CBR [5] (expect for high oil inclusions), and compression index ▪ Decrease in the optimum moisture content, coefficient of permeability, angle of internal friction (a modest decrease up to about 2° for triaxial tests, and up to 7° for direct shear tests), and stiffness
Ratnaweera and Meegoda (2006)	SM [6] CL [7] CH	Acetone Glycerol Propanol	▪ Increase in the ductility (for the CL and CH soils), and drained shear strength (peak and residual) in some cases for the SM soil ▪ Decrease in both the unconfined compressive strength and stiffness with increase in pore–fluid viscosity for the CL and CH soils
Khamehchiyan et al. (2007)	SP SM CL	Crude oil	▪ Increase in the angle of internal friction (for the CL soil), and cohesion (for the SP and SM soils with a minor increase) ▪ Decrease in the liquid and plastic limits (for the CL soil), maximum dry unit weight, optimum moisture content, coefficient of permeability, unconfined compressive strength (except for low inclusions of crude oil in the CL soil), angle of internal friction (for the SP and SM soils), and cohesion (for the CL soil)
Moavenian and Yasrobi (2008)	CH	Ethylene glycol Toluene	▪ Increase in the plastic limit, while the samples contaminated with pure ethylene glycol and toluene displayed a non–plastic behavior ▪ Decrease in the liquid limit, plasticity index, and swelling potential
Singh et al. (2008)	CL CH	Diesel Gasoline Kerosene UEO [8]	▪ Increase in both the liquid limit and the compression index (expect for the samples contaminated with kerosene) ▪ Decrease in the coefficient of consolidation
Olgun and Yıldız (2010)	CH	Acetic acid Ethanol IPA [9] Methanol	▪ Increase in the coefficient of permeability, angle of internal friction, and cohesion (in the case of low contaminant to water ratios, a minor increase in the undrained shear strength was observed) ▪ Decrease in the liquid limit, plasticity index, compression index (minor in the case of acetic acid), and swelling index
Di Matteo et al. (2011)	MH [10]	EGB [11]	▪ Decrease in both the liquid limit and compression index with increase in the dielectric constant and absolute viscosity of the pore–fluid (in the case of water as the pore–fluid, however, both the liquid limit and the compression index were observed to be significantly lower than the contaminated samples)
Kermani and Ebadi (2012)	CL	Crude oil	▪ Increase in the liquid and plastic limits, maximum dry unit weight, angle of internal friction, and compressibility characteristics ▪ Decrease in the optimum moisture content, and cohesion
Khosravi et al. (2013)	CL	Gas oil	▪ Increase in the liquid limit and plasticity index (except for high inclusions of gas oil), unconfined compressive strength, stiffness, and cohesion ▪ Decrease in the plastic limit, compression index, swelling index, and angle of internal friction (a minor decrease was observed for the majority of cases)
Estabragh et al. (2014)	CL CH	Ethanol Glycerol	▪ Increase in the compression index for the slurry samples, and pre–consolidation pressure for the pre–consolidated slurry samples (the increase in pre–consolidation pressure was minor in the case of

			glycerol) ▪ Decrease in the compression index for the pre–consolidated slurry samples
Liu et al. (2015)	CL	Diesel oil	▪ Decrease in the liquid and plastic limits (accompanied by a minor increase in the plasticity index), swelling pressure, unconfined compressive strength, and stiffness
Estabragh et al. (2016a)	CL	Ethanol Glycerol	▪ Increase in the pre–consolidation pressure (minor increase in the case of glycerol), angle of internal friction, stiffness, and slope of the critical state line ▪ Decrease in the compression index
Estabragh et al. (2016b)	CL	Glycerol	▪ Increase in the maximum dry unit weight, and ductility ▪ Decrease in the liquid and plastic limits, plasticity index, optimum moisture content, unconfined compressive strength, and stiffness
Estabragh et al. (2016c)	CL	MEG [12]	▪ Increase in the maximum dry unit weight, and ductility ▪ Decrease in the liquid and plastic limits, plasticity index, optimum moisture content, unconfined compressive strength, and stiffness
Nasehi et al. (2016)	SP ML CL	Gas oil	▪ Increase in the liquid and plastic limits (accompanied by minor variations in the plasticity index), and cohesion ▪ Decrease in the maximum dry unit weight, optimum moisture content, unconfined compressive strength (except for low inclusions of gas oil in the CL soil), and angle of internal friction
Estabragh et al. (2017)	CL	MTBE [13]	▪ Increase in the ductility ▪ Decrease in the unconfined compressive strength, and stiffness

[1] increase or decrease in soil properties as a result of contamination or increase in degree of contamination (i.e. contaminant to dry soil mass ratio); [2] silt with low plasticity; [3] clay with high plasticity; [4] poorly–graded sand; [5] California bearing ratio; [6] silty sand; [7] clay with low plasticity; [8] used engine oil; [9] isopropyl alcohol; [10] silt with high plasticity; [11] ethanol–gasoline blends; [12] mono–ethylene glycol; and [13] methyl tert–butyl ether.

Table 2. Mechanical properties of the soils

Properties	**Soil A**	**Soil B**	**Standard designation**
Specific gravity, G_s	2.71	2.76	ASTM D854
Clay (<2 μm) (%)	29.70	41.15	ASTM D422
Silt (2–75 μm) (%)	54.60	42.75	
Sand (0.075–4.75 mm) (%)	14.25	16.10	
Liquid limit, *LL* (%)	43.12	85.30	ASTM D4318
Plastic limit, *PL* (%)	19.85	26.05	
Plasticity index, *PI* (%)	23.27	59.25	
USCS soil classification	CI	CH	ASTM D2487
Optimum water content, ω_{opt} (%)	19.05	23.40	ASTM D698
Maximum dry unit weight, γ_{dmax} (kN/m^3)	16.71	14.95	
Unconfined compressive strength, q_u (kPa) [1]	426.82	359.70	ASTM D2166

[1] unconfined compressive strength at optimum water content and maximum dry unit weight (i.e. initial void ratio of e_0=0.591 and 0.811 for soils A and B, respectively).

Table 3. Physical and chemical properties of the contaminant agents (at 25 °C)

Contaminant	**Glycerol**	**Ethanol**	**Ethylene glycol**
Chemical formulation	$C_3H_8O_3$	C_2H_6O	$C_2H_6O_2$
Mass density, ρ (kg/m^3)	1097.10	944.80	1077.40
Absolute viscosity, μ_c (cP) [1]	4.310	2.148	1.181
Dielectric constant, D	67.10	54.82	65.40
Square root of the dielectric constant, $D^{0.5}$	8.19	7.40	8.09
Electrical conductivity, EC (dS/m)	8.40×10^{-3}	8.40×10^{-3}	8.40×10^{-3}

[1] 1 cP (centipoise)=10^{-3} Pa.s (pascal–second).

Accepted manuscript
doi: 10.1680/jenge.18.00018

Table 4. Mechanical properties of the prepared samples

Soil	Contaminant	C_c (%)	*LL* (%)	*PL* (%)	*PI* (%)	ω'_{opt} (%)	γ_{dmax} (kN/m^3)
Soil A	—	0	43.12	19.85	23.27	19.05	16.71
	Ethylene glycol	2	42.75	19.70	23.05	19.01	16.60
		4	42.05	18.70	23.35	18.80	17.02
		6	40.65	18.50	22.15	18.10	17.45
		8	38.67	17.50	21.17	17.44	17.55
	Ethanol	2	41.73	19.30	22.43	19.20	16.80
		4	40.11	18.10	22.01	18.90	16.60
		6	39.47	18.20	21.27	17.52	16.50
		8	38.03	17.20	20.83	16.56	16.90
	Glycerol	2	40.53	18.57	21.96	19.82	16.70
		4	38.86	17.62	21.24	18.50	17.35
		6	37.72	17.01	20.71	17.20	17.62
		8	36.27	16.23	20.04	15.40	17.85
Soil B	—	0	85.30	26.05	59.25	23.40	14.95
	Ethylene glycol	2	83.61	25.85	57.76	22.35	15.10
		4	81.90	25.22	56.68	21.75	15.40
		6	79.25	24.14	55.11	21.11	15.75
		8	77.91	23.72	54.19	20.35	16.05
	Ethanol	2	81.15	24.90	56.25	21.11	14.80
		4	78.30	23.65	54.65	20.34	14.90
		6	77.62	22.80	54.82	18.65	15.00
		8	74.52	21.31	53.21	18.80	15.50
	Glycerol	2	79.01	23.81	55.20	20.51	15.10
		4	76.85	22.52	54.33	19.33	15.80
		6	73.52	21.25	52.27	17.70	16.18
		8	70.31	19.83	50.48	17.04	16.80

C_c=degree of contamination (=$W_c/W_s\times100$); *LL*=liquid limit; *PL*=plastic limit; *PI*=plasticity index (=*LL*–*PL*); ω'_{opt}=optimum moisture content (=[W_c+W_w]/$W_s\times100$); and γ_{dmax}=maximum dry unit weight.

Accepted manuscript
doi: 10.1680/jenge.18.00018

Table 5. Summary of the regression analysis outputs with respect to the proposed dimensional models, i.e. Equation (10) for q_u, and Equation (11) for E

Soil	Variable	α_0 or β_0	α_1 or β_1	α_2 or β_2	R^2	RMSE (kPa)	NRMSE (%)	MAPE (%)
A	q_u (Pa)	9.41×10^3	9.93×10^3	–0.763	0.985	8.52×10^0	3.86	2.29
	E (Pa)	4.17×10^5	9.12×10^5	–1.080	0.989	6.76×10^2	3.11	3.84
B	q_u (Pa)	4.36×10^3	6.81×10^3	–1.044	0.963	1.33×10^1	5.80	5.31
	E (Pa)	1.17×10^5	3.80×10^5	–1.885	0.981	5.41×10^2	3.98	7.48

Accepted manuscript
doi: 10.1680/jenge.18.00018

Table 6. Summary of the sensitivity analysis results for μ_c and C_c with respect to the proposed dimensional models, i.e. Equation (10) for q_u, and Equation (11) for E.

x_i [1]	Soil	y_i [2]	$\frac{1}{n}\sum_{j=1}^{n}\left\|\frac{\partial y_i}{\partial x_i}\right\|_j$	$\sigma(x_i)$	$\sigma(y_i)$	$S(x_i)$	$P(x_i)^+$	$P(x_i)^-$	$\eta(x_i)^+$	$\eta(x_i)^-$
μ_c	A	q_u (Pa)	2.93×10^{7}	1.37×10^{-3}	6.50×10^{4}	0.62	0	100	0.62	0
	B		2.98×10^{7}	1.37×10^{-3}	6.24×10^{4}	0.65	0	100	0.65	0
	A	E (Pa)	2.83×10^{9}	1.37×10^{-3}	5.85×10^{6}	0.66	0	100	0.66	0
	B		1.67×10^{9}	1.37×10^{-3}	3.22×10^{6}	0.71	0	100	0.71	0
C_c	A	q_u (Pa)	1.37×10^{6}	2.34×10^{-2}	6.50×10^{4}	0.49	0	100	0.49	0
	B		1.42×10^{6}	2.34×10^{-2}	6.24×10^{4}	0.53	0	100	0.53	0
	A	E (Pa)	1.35×10^{8}	2.34×10^{-2}	5.85×10^{6}	0.54	0	100	0.54	0
	B		8.30×10^{7}	2.34×10^{-2}	3.22×10^{6}	0.60	0	100	0.60	0

[1] independent variables; and [2] dependent variable.

Accepted manuscript
doi: 10.1680/jenge.18.00018

Figure 1. Location of the contaminated mixtures on Cassgrande's plasticity chart: **(a)** Soil A; and **(b)** Soil B

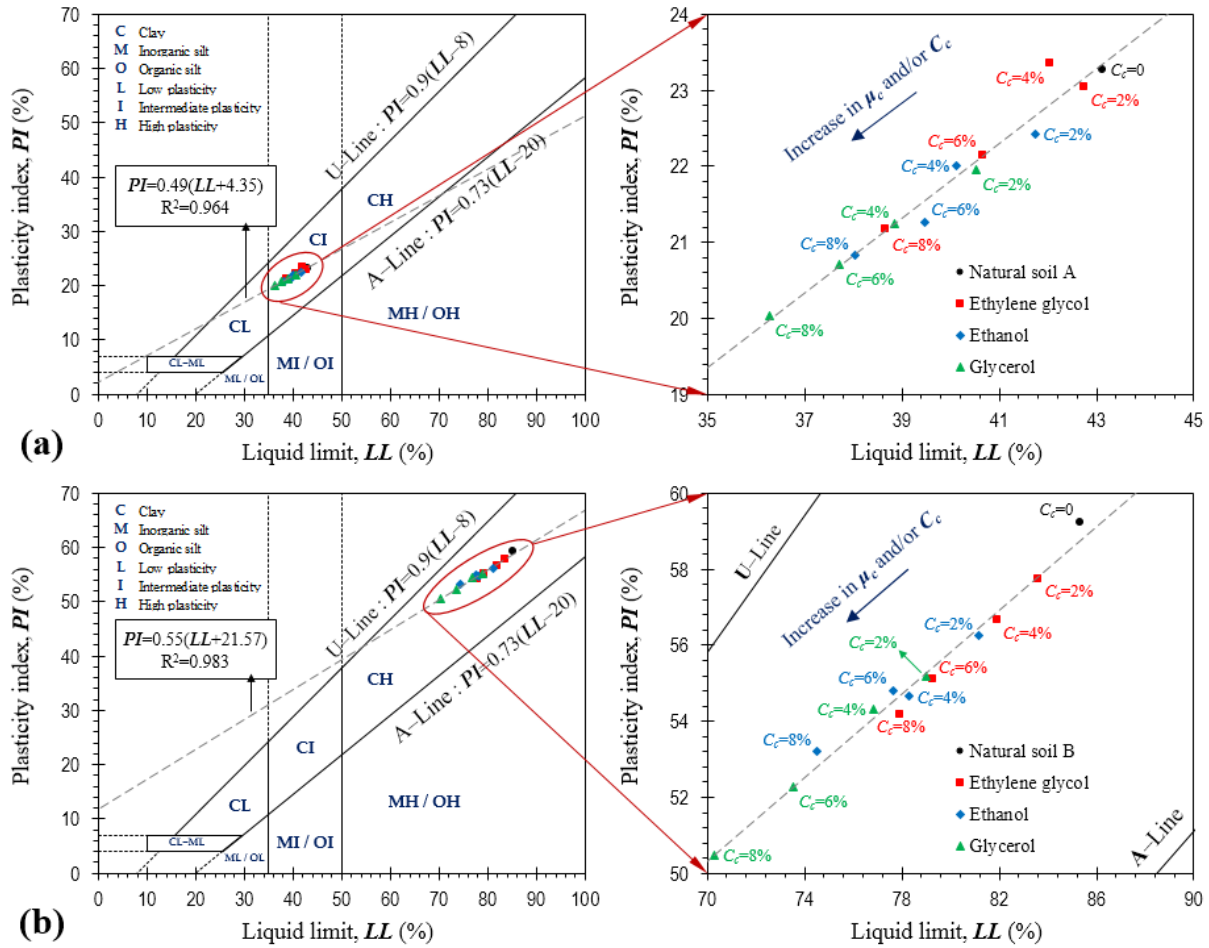

Accepted manuscript
doi: 10.1680/jenge.18.00018

Figure 2. Stress–strain curves for the natural soil and various ethanol–contaminated samples: **(a)** Soil A; and **(b)** Soil B

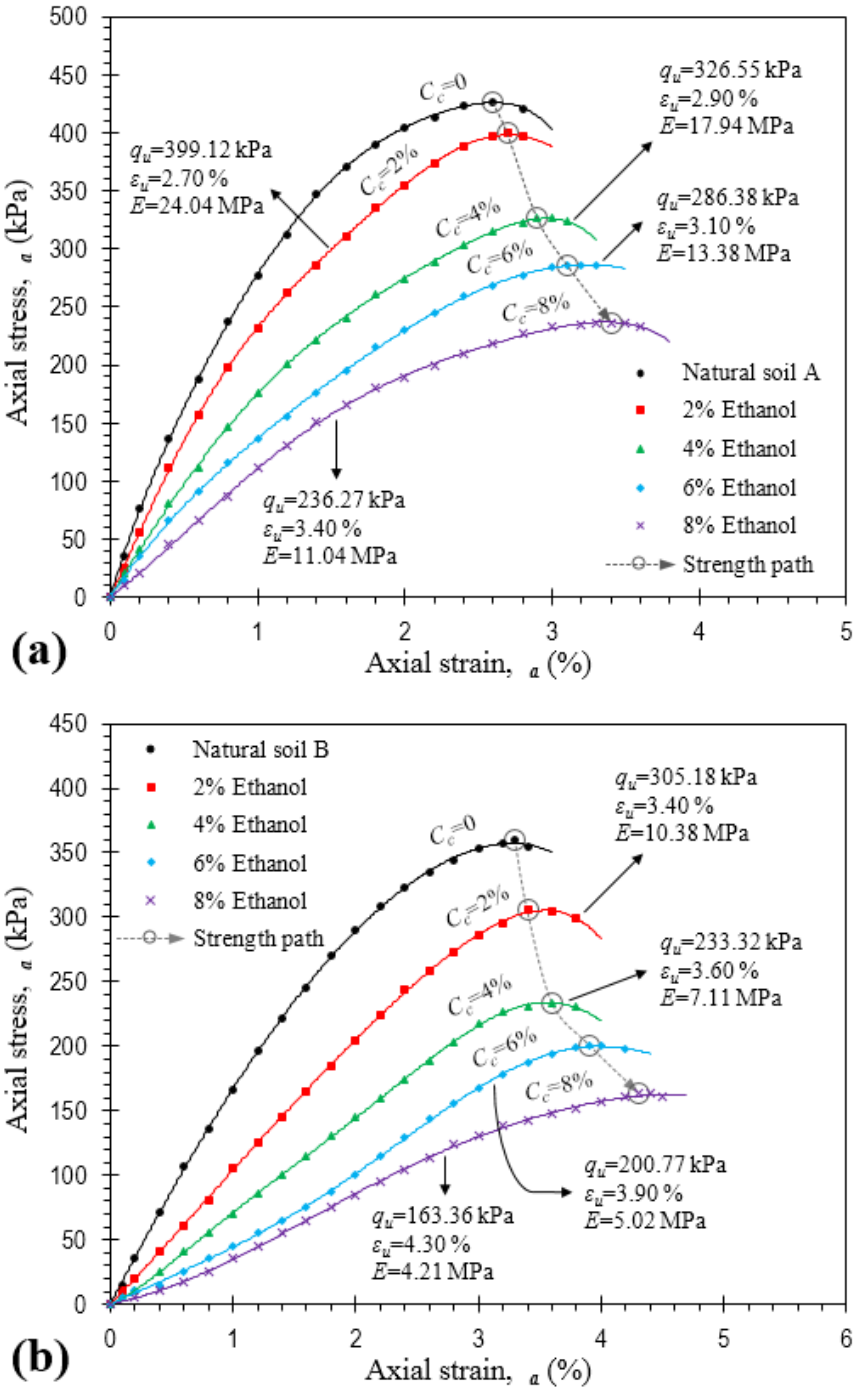

Accepted manuscript
doi: 10.1680/jenge.18.00018

Figure 3. Stress–strain curves for the natural soil and the samples contaminated with C_c=6% glycerol, ethanol and ethylene glycol: **(a)** Soil A; and **(b)** Soil B

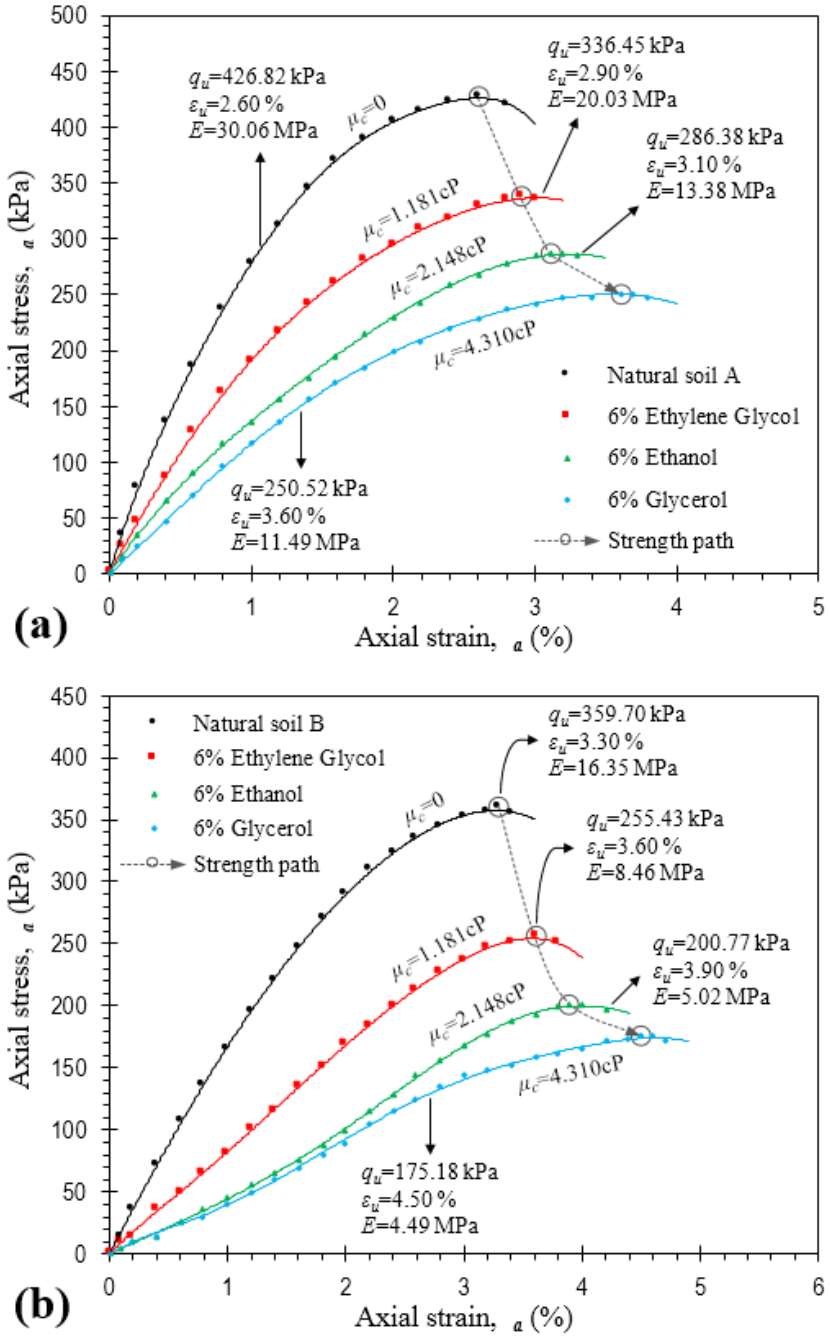

Accepted manuscript
doi: 10.1680/jenge.18.00018

Figure 4. Strength properties against C_c for soil A: **(a)** Unconfined compressive strength q_u; **(b)** Modulus of elasticity E; and **(c)** Axial strain at failure ε_u

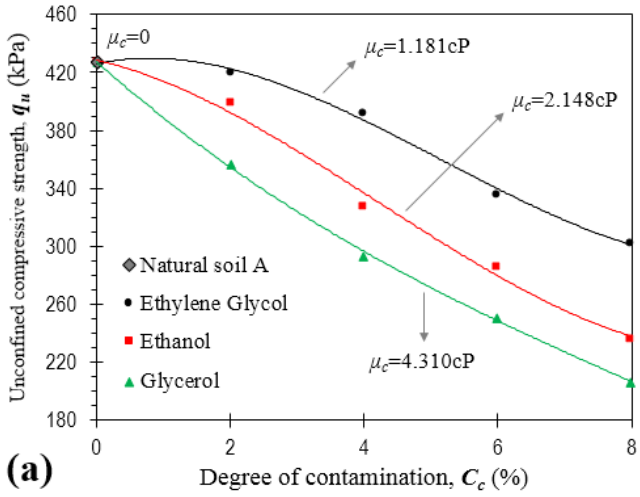

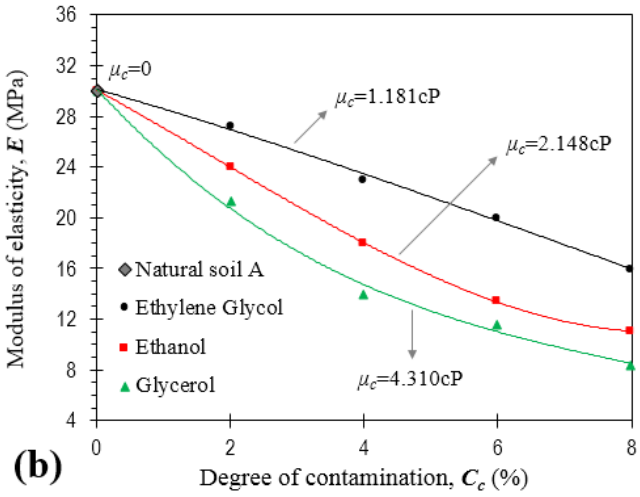

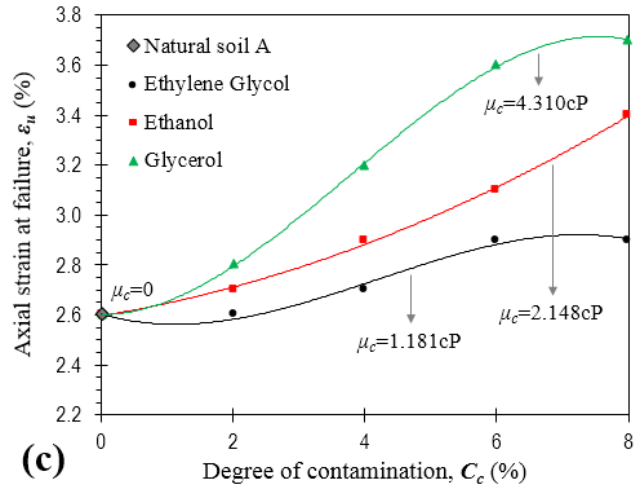

Accepted manuscript
doi: 10.1680/jenge.18.00018

Figure 5. Strength properties against C_c for soil B: **(a)** Unconfined compressive strength q_u; **(b)** Modulus of elasticity E; and **(c)** Axial strain at failure ε_u

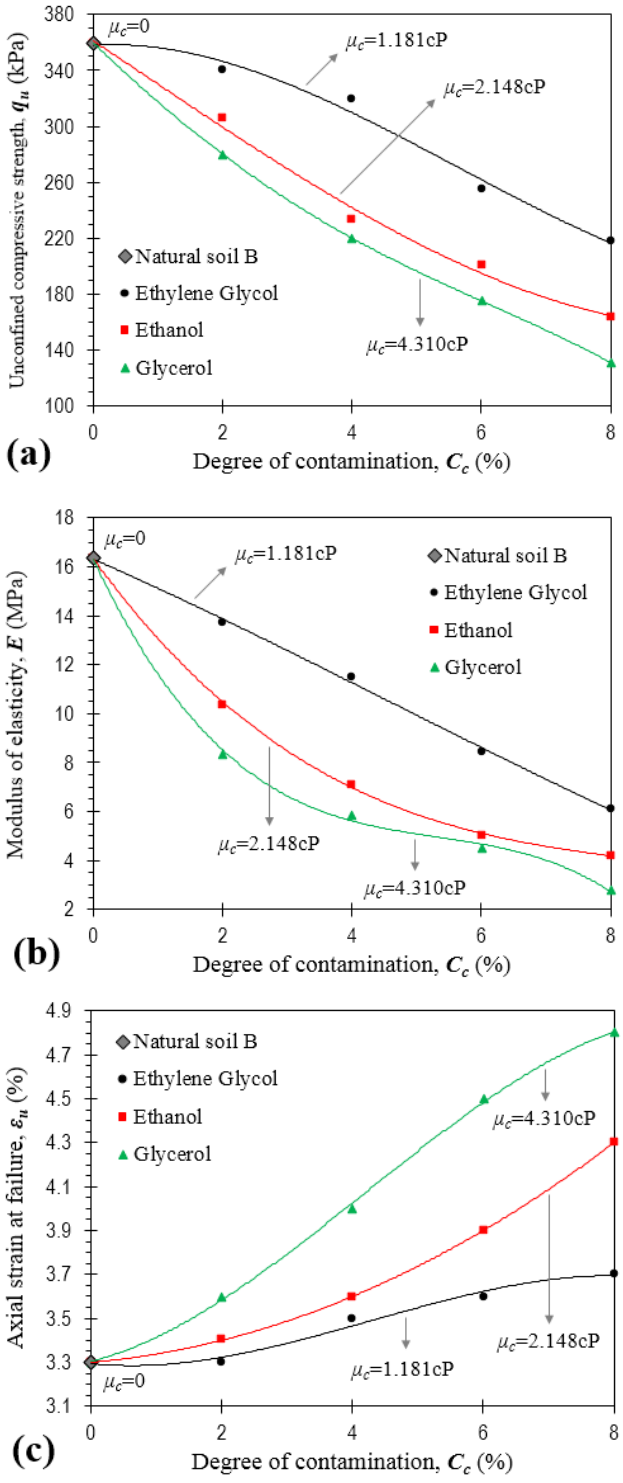

Accepted manuscript
doi: 10.1680/jenge.18.00018

Figure 6. Variations of the dependent π term against the independent π terms: **(a)** π_0–π_1; **(b)** π_0–π_2; and **(c)** π_0–π_3

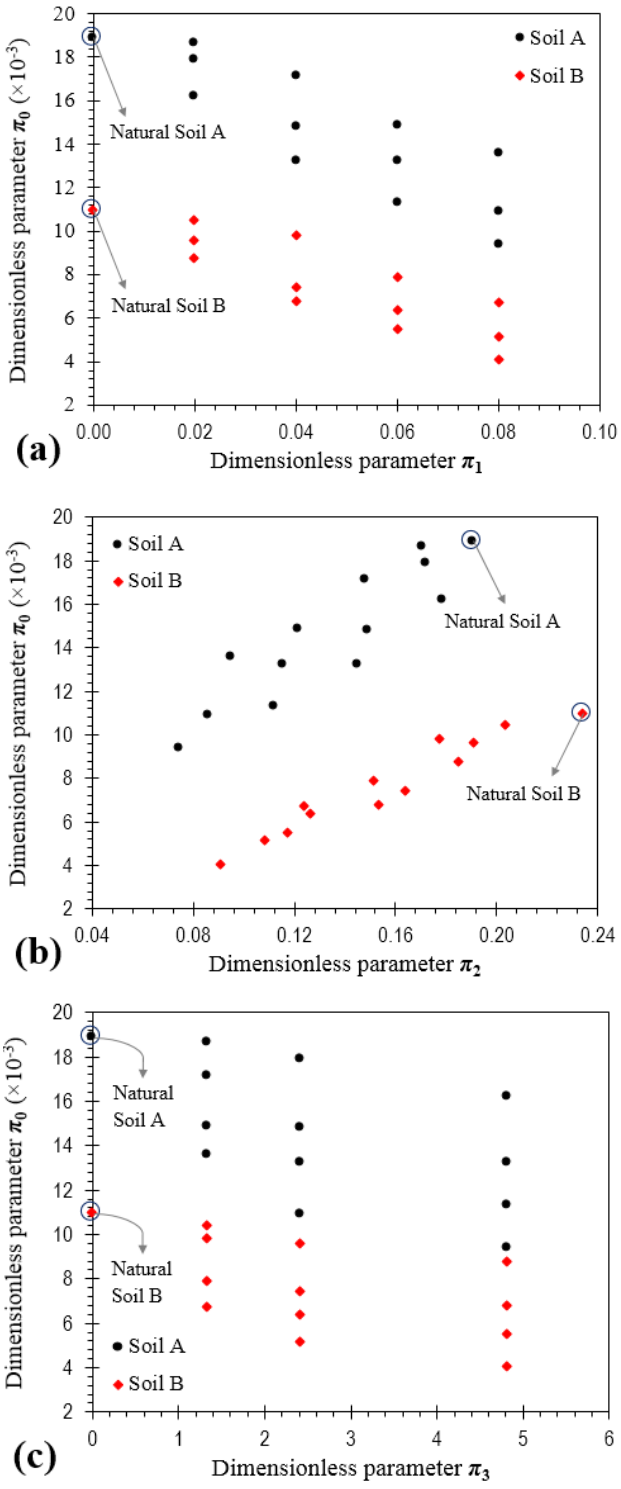

Accepted manuscript
doi: 10.1680/jenge.18.00018

Figure 7. Variations of π_0 against the dimensionless viscosity number μ^*: **(a)** q_u data; and **(b)** E data

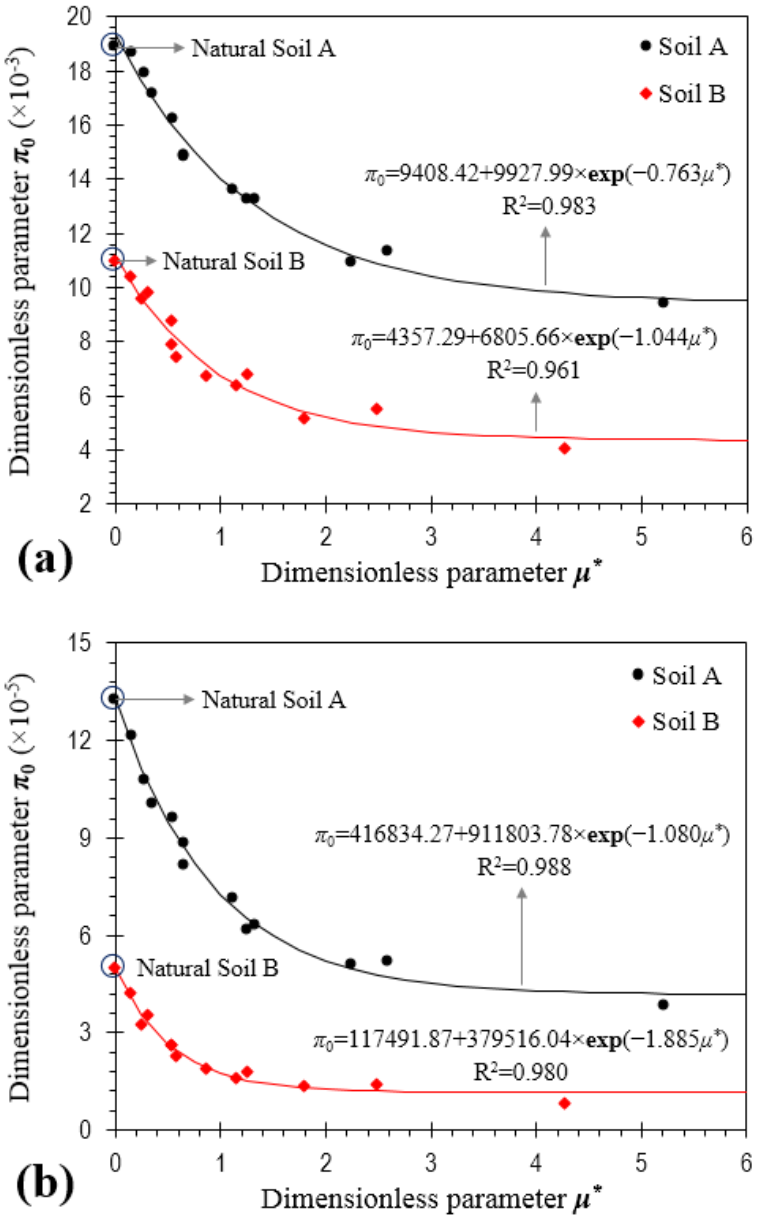

Accepted manuscript
doi: 10.1680/jenge.18.00018

Figure 8. Actual versus predicted data with respect to the proposed dimensional models: **(a)** q_u or Equation (10); and **(b)** E or Equation (11)